Protoplasma (2017) 254:2017–2034
DOI 10.1007/s00709-017-1089-9

ORIGINAL ARTICLE

Morpho-histological, histochemical, and molecular evidences related to cellular reprogramming during somatic embryogenesis of the model grass *Brachypodium distachyon*

Evelyn Jardim Oliveira[1] · Andréa Dias Koehler[1] · Diego Ismael Rocha[2] · Lorena Melo Vieira[1] · Marcos Vinícius Marques Pinheiro[1] · Elyabe Monteiro de Matos[1] · Ana Claudia Ferreira da Cruz[1] · Thais Cristina Ribeiro da Silva[1] · Francisco André Ossamu Tanaka[3] · Fabio Tebaldi Silveira Nogueira[4] · Wagner Campos Otoni[1]

Received: 20 November 2016 / Accepted: 13 February 2017 / Published online: 13 March 2017

Abstract The wild grass species *Brachypodium distachyon* (L.) has been proposed as a new model for temperate grasses. Among the biotechnological tools already developed for the species, an efficient induction protocol of somatic embryogenesis (SE) using immature zygotic embryos has provided the basis for genetic transformation studies. However, a systematic work to better understanding the basic cellular and molecular mechanisms that underlie the SE process of this grass species is still missing. Here, we present new insights at the morpho-histological, histochemical, and molecular aspects of *B. distachyon* SE pathway. Somatic embryos arose from embryogenic callus formed by cells derived from the protodermal-dividing cells of the scutellum. These protodermal cells showed typical meristematic features and high protein accumulation which were interpreted as the first observable steps towards the acquisition of a competent state. Starch content decreased along embryogenic callus differentiation supporting the idea that carbohydrate reserves are essential to morphogenetic processes. Interestingly, starch accumulation was also observed at late stages of SE process. Searches in databanks revealed three sequences available annotated as *BdSERK*, being two copies corresponding to *SERK1* and one showing greater identity to *SERK2*. In silico analysis confirmed the presence of characteristic domains in a *B. distachyon Somatic Embryogenesis Receptor Kinase* genes candidates (*BdSERKs*), which suggests *SERK* functions are conserved in *B. distachyon.* In situ hybridization demonstrated the presence of transcripts of *BdSERK*1 in all development since globular until scutellar stages. The results reported in this study convey important information about the morphogenetic events in the embryogenic pathway which has been lacking in *B. distachyon*. This study also demonstrates that *B. distachyon* provides a useful model system for investigating the genetic regulation of SE in grass species.

Keywords Cellular competency · Grass · Histology · In situ hybridization · *SERK* genes · Somatic embryogenesis

Handling Editor: Peter Nick

Electronic supplementary material The online version of this article (doi:10.1007/s00709-017-1089-9) contains supplementary material, which is available to authorized users.

✉ Fabio Tebaldi Silveira Nogueira
ftsnogue@usp.br

✉ Wagner Campos Otoni
wcotoni@gmail.com

[1] Laboratório de Cultura de Tecidos/BIOAGRO, Departamento de Biologia Vegetal, Universidade Federal de Viçosa, Avenida P. H. Rolfs s/n, 36570-900 Viçosa, MG, Brazil

[2] Instituto de Biociências, Universidade Federal de Goiás, Regional Jataí, BR 364, km 195, 75801-615 Jataí, GO, Brazil

[3] Departamento de Fitopatologia e Nematologia, Universidade de São Paulo/ESALQ, Av. Pádua Dias, 13418-900 Piracicaba, SP, Brazil

[4] Laboratorio de Genética Molecular do Desenvolvimento Vegetal (LGMDV), Universidade de São Paulo/ESALQ, Av. Pádua Dias, 13418-900 Piracicaba, SP, Brazil

Introduction

Over the past decade, *Brachypodium distachyon* has been proposed as a model species for molecular genetics researches of temperate grasses and cereals (Draper et al. 2001; Vogel and

Bragg 2009; Brkljacic et al. 2011; Girin et al. 2014; Fitzgerald et al. 2015; Kellogg 2015; Vogel 2016). *B. distachyon* is an ideal species for functional genomic studies of grass, because of its easy growth requirements, small stature, rapid life cycle, small genome, and self-pollination (Opanowicz et al. 2008; Kellogg 2015; Vogel 2016). In addition, important genomic resources have been developed for *B. distachyon* as transformation protocols, large expressed sequence tag (EST) databases, tools for forward and reverse genetic screens, highly refined cytogenetic probes, germplasm collections, and recently, a complete genome sequence has been generated (Vain 2011; Brkljacic et al. 2011; Vogel 2016).

Functional genomics studies require from any model plant species appropriated transformation and in vitro regeneration systems. An efficient tissue culture protocol to induce somatic embryogenesis (SE) from immature zygotic embryos has been established for *B. distachyon* (Ye and Tao 2008). SE is the development program by which somatic cells develop into differentiated somatic embryos under appropriate conditions. These somatic embryos differentiate into whole plants by passing through the zygotic embryo stages of sexual fertilization (Zimmerman 1993; Von Arnold et al. 2002; Yang and Zhang 2010; Rocha and Dornelas 2013; De Fillipis 2014; Smertenko and Bozhkov 2014). SE plays a very important role in in vitro plant regeneration of various cereal and grass species (Ozias-Akins and Vasil 1982; Vasil et al. 1985; Brisibe et al. 1993; Taylor and Vasil 1996; Mariani et al. 1998; Wrobel et al. 2011). When integrated with conventional breeding programs and molecular and genetic engineering techniques, SE provides a valuable tool to enhance genetic improvement of crop species (Quiroz-Figueroa et al. 2006; De Fillipis 2014). However, genetic engineering or mutagenesis techniques cannot be successfully achieved if the basic knowledge underlying the morphogenesis processes is not well understood (Fortes and Pais 2000; Verdeil et al. 2007; Yang and Zhang 2010).

During early stages of SE induction, a given somatic cell responds to the environmental conditions and growth regulators supplement acquiring competence to assume a new developmental fate. After that, the competent cell or tissue become determined (committed) to form the somatic embryos (Yang and Zhang 2010). Descriptions of the cellular changes occurring during the transition SE pathway and histodifferentiation of somatic embryos have been reported for many eudicot species (Moura et al. 2010; Wrobel et al. 2011; Pan et al. 2011; Rocha et al. 2012, 2016). It has been shown for eudicots that there are particular cellular and histological features which allow the recognition of the transition from the somatic to the embryogenic state during this developmental process (Verdeil et al. 2007; Kurczyńska et al. 2012; Betekhtin et al. 2016; Rocha et al. 2016). On the other hand, in monocots the cellular events underlying the acquisition of competence and the transition of somatic cells to the embryogenic cell state are poorly elucidated (Lenis-Manzano et al. 2010; Delporte et al. 2014; Cabral et al. 2015).

The cellular reprogramming that occurs throughout the SE developmental program is closely related to alterations in gene expression (Karami et al. 2009; Yang and Zhang 2010; Rocha and Dornelas 2013; De Fillipis 2014). The *Somatic Embryogenesis Receptor Kinase* (*SERK*) gene is among the genes involved in the induction of SE and has been used to monitor the transition from somatic cells to callus proliferation and embryogenic cells formation (Schmidt et al. 1997; Hecht et al. 2001; Somleva et al. 2000; Nolan et al. 2003; Santa-Catarina et al. 2004; Singla et al. 2008; Pérez-Nuñéz et al. 2009; Nolan et al. 2009; Savona et al. 2012; Steiner et al. 2012; Pilarska et al. 2016; Rocha et al. 2016). SERK is a leucine-rich repeat (LRR) transmembrane protein kinase that enhances the ability of the apical meristem in *Arabidopsis* to form somatic embryos when *SERK* genes are overexpressed (Hecht et al. 2001). *SERK* gene was found to be expressed during callus differentiation, and expressed from proembryogenic mass formation to the globular stage during SE of many eudicot species (see review aan den Toorn et al. 2015). Homologs of the *SERK* genes were also isolated from some monocots species as *Zea mays* (Baudino et al. 2001), *Oryza sativa* (Hu et al. 2005), *Triticum aestivum* (Singla et al. 2008), and *Secale cereale* (Gruszczyńska and Rakoczy-Trojanowska 2011). However, in contrast to the knowledge available regarding molecular mechanisms involved in the control of eudicots-SE, the expression pattern of *SERK* genes has not been extensively studied in monocots-SE.

In this work, we described in great details at the cellular and molecular levels the mechanisms related to SE induction of the grass model *B. distachyon*. We characterized the histological and histochemical changes involved in SE induction and verify the dynamics of expression of *SERK* gene throughout the embryogenic pathway obtained from immature zygotic embryos of *B. distachyon*. The findings of this study provide a useful model system for investigating the genetic regulation of SE in grass species.

Materials and methods

Plant material

B. distachyon (line Bd21) was provided by Dr. John Vogel from the US Department of Agriculture. Selfed seeds of *B. distachyon* (line Bd21) were sown in 8-cm plastic pots containing a compost:vermiculite mixture (2:1) and stratified at 4 °C for 1 week after sowing. Plants were grown in controlled growth chambers under 20 h light:4 h dark photoperiod at 23 °C with cool-white fluorescent lighting at a level of

150 μE m^{-2} s^{-1}, until maturation to generate a seed stock to initiate experiments.

Production of embryogenic callus and plant regeneration

Immature seeds obtained around 8–12 weeks after potting were sterilized for 30 s with 20 mL of 70% ethanol in a capped sterile Petri dish. Ethanol was drained and seeds were rinsed with sterilized deionized water. Seeds were placed in 20 mL of 1.3% sodium hypochlorite solution for 4 min and then rinsed three times with sterilized deionized water. Lemma (upper glume) was removed from immature seeds and immature embryos were dissected out from seeds with watery to milky endosperm with a fine forceps under aseptic conditions in a laminar flow hood using a stereo microscope.

Twenty immature embryos were cultured with the scutellum facing up in 9-cm-diameter Petri dishes containing 25 mL of induction medium [Murashige and Skoog (MS) salts (Murashige and Skoog 1962), 4 g L^{-1} of Fe-ethylenediaminetetraacetate (Fe-EDTA), 30 g L^{-1} of sucrose, 2.5 mg L^{-1} of 2,4-dichlorophenoxyacetic acid, 0.6 mg L^{-1} of $CuSO_4$, and 2 g L^{-1} of Phytagel (Sigma Aldrich®); pH 5.8] at 25 °C in the dark. Filter-sterilized vitamin M5 [2 mg L^{-1} of glycine, 0.4 mg L^{-1} of nicotinic acid, 0.4 mg L^{-1} of pyridoxine-HCl, 0.5 mg L^{-1} of thiamine-HCl, and 40 mg L^{-1} of cysteine] was added after autoclaving. The elongated coleoptiles were excised when they appeared, during the first 2–3 days of culture. After 3–4 weeks, embryogenic calli with a creamy color and pearly surface were fragmented in 2–4 pieces and transferred (20 callus pieces per plate) onto regeneration medium (MS salts, Fe-EDTA, 30 g L^{-1} of sucrose, 0.2 mg L^{-1} of kinetin, vitamins M5, 2 g L^{-1} of Phytagel; pH 5.8) for 2–3 weeks at 25 °C under 16-h photoperiod. Shoots (rooted or not) were transferred to jars containing germination medium (40% MS salts, Fe-EDTA, 10 g L^{-1} of sucrose, vitamins B5, 2 g L^{-1} of Phytagel, 6 g L^{-1} of agar; pH 5.8). Shoots were cultured for 2–3 weeks at 23 °C under 16-h photoperiod. Regenerated plantlets were potted in plastic pots containing a wet compost mixture (3:1 Plantmax®:vermiculite). Plants were grown in a Controlled Environment Room (Forma Scientific) at 23 °C with a 20-h light photoperiod for 5–6 weeks.

Microscopy sample preparation

For anatomical and histochemical characterizations of the SE process, immature seeds obtained around 15 days after anthesis and immature zygotic embryos were collected every day from 1 to 6 days after culture in induction medium, then at days 8, 12, and 21. Samples were fixed in Karnovsky's solution (Karnovsky 1965).

Light microscopy and histochemical characterization

For the anatomical studies, fixed immature embryo samples were dehydrated in a graded ethanol series and embedded in methacrylate (Historesin, Leica Instruments, Germany). Longitudinal sections (5 μm in thickness) were obtained with an automated advance rotary microtome (RM2155, Leica Microsystems Inc., USA) and stained with toluidine blue at pH 4.4 (O'Brien and McCully 1981) for structural characterization, Xylidine Ponceau (XP) for total protein quantification (Vidal 1977), periodic acid–Schiff's reagent (PAS) for the quantification of polysaccharides with vicinal glycol groups (Feder and O'Brien 1968), and Sudan black B (Pearse 1980) for total lipid quantification. Images were captured on a light and fluorescence microscope (Olympus AX70TRF, Olympus Optical, Japan) coupled with a digital camera (AxioCam HR, Zeiss).

Scanning electron microscopy

Fixed samples were dehydrated with an increasing acetone series, subjected to critical point drying (CPD 030, Bal-Tec, Balzers, Germany), and coated with gold (SCD 050, Bal-Tec, Balzers, Germany). Samples were analyzed on a scanning electron microscope (LEO 435-VP, Cambridge, England) and all images were processed digitally.

Transmission electron microscopy

Fixed samples were post fixed with 1% of osmium tetroxide in 0.05-M phosphate buffer, dehydrated in an increasing acetone series of acetone, and embedded in epoxy resin (Spurr 1969). Ultrathin sections (70 nm in thickness) were obtained with an ultramicrotome (Leica UC6, Leica Microsystems Inc., USA) and contrasted with uranyl acetate and lead citrate (Reynolds 1963). Research and documentation were performed with a transmission electron microscope (EM900, Zeiss, Germany) at 50 kV.

Identification and characterization of *SERK* genes in *B. distachyon*

To identify homologs of *SERK* genes of *B. distachyon* and other species used in this study, research was carried out in Phytozome (https://phytozome.jgi.doe.gov) and NCBI (https://www.ncbi.nlm.nih.gov/) databases. The sequences obtained were compared with members of the SERK family of other species using the BLASTP tool against the non-redundant databank of NCBI.

Information on the position and conservation of the structural domains were searched from CDD Conserved Domain database (NCBI) and Pfam 30.0 (pfam.xfam.org), and demonstrated through multiple sequence alignment (MSA)

of the predicted amino acid sequences with other grass SERK protein sequences, available at the Genbank. The MSA was obtained by ClustalW in the Bioedit 7.2 software. The signal peptide prediction was performed by SignalP 4.1 Server (http://www.cbs.dtu.dk/services/SignalP) (Petersen et al. 2011). The phylogenetics relationship of the *BdSERK* sequences was investigated by building a rooted phylogenetics tree with other 65 homologs from different taxonomic plant groups and 4 non-SERK kinase proteins used as external group (aan den Toorn et al. 2015), using MEGA (Molecular Evolutionary Genetics Analysis) software version 7.0 (Kumar et al. 2016) by Neighbor-Joining method (NJ) (Saitou and Nei 1987) and bootstrap test with 1000 replicates.

Additionally, a score of conservation for each amino acids was determined using the Consurf Server (http://consurf.tau.ac.il/). The results were plotted onto crystal structures (PDB:4 LSC) for SERK1 extracellular domain (Santiago et al. 2013; aan den Toorn et al. 2015) available at PDB (Protein Data Bank - www.wwpdb.org). The analysis was performed from alignment of the aforementioned 65 SERK protein homologs (aan den Toorn et al. 2015) using BdSERK1 (Bradi5g12227) and BdSERK2 (Bradi3g15660) as query sequences. The molecular graphics and analysis were performed with PyMOL Viewer software version 0.99rc6.

Spatial and temporal localization of *SERK* transcripts by situ hybridization

Samples were collected at 0, 2, 12, 14, and 21 days in induction medium and immediately immersed into fixing solution (4% of paraformaldehyde and 0.25% of glutaraldehyde in sodium phosphate buffer at 0.01 M; pH 7.2). Samples were subjected to vacuum for 1 h at room temperature and then kept at 4 °C for 16 h. Next, samples were dehydrated in an ethanol series, embedded in BMM (butyl-methyl-methacrylate, Sigma Aldrich®) resin, polymerized for 48 h at 4 °C under ultraviolet light 815 2537 A° (15 W), and stored at −20 °C.

Sections of 4 μm were produced using an automated advance rotary microtome (RM2155, Leica Microsystems Inc., USA) and placed in water droplets on RNase-free Fisherbrand® silane-treated slides microscope (Fisher Scientific). The sections were dried in a heating plate at 60 °C and stored at 4 °C until used. Prior to hybridization, the BMM was removed from the sections by consecutive 10-min washes in 100% acetone, acetone:DEPC-treated water (1:1, *v*/*v*), and twice in DEPC-treated water.

A fragment of 766 bp of BdSERK1 obtained from cDNA amplification of embryogenic callus with 21 days of culture was cloned into pGEM T Easy vector (Promega), and used as a template for constructing antisense and sense probes. The probes were labeled with digoxigenin (DIG-UTP) using the DIG RNA Labeling Kit (SP6/T7) according to manufacturer's (Roche Applied Science) recommendations.

For hybridization reaction, 60 ng of probe and 60 ng of yeast tRNA (Gibco BRL®) were denatured at 80 °C for 5 min and added to 100 mL of hybridization buffer (10 mM of Tris-HCl at pH 7.5, 300 mM of NaCl, formamide 50%, 1 mM of EDTA at pH 8.0, 1X Denhardt's solution). For hybridization, 100 μL of hybridization solution was placed onto each slide, which was covered with Parafilm®. The slides were incubated in a moist chamber at 42 °C in the dark for approximately 16 h. After hybridization, the slides were washed in 4X, 2X, 0.5X, and 1X SSC solutions (20X SSC = 3 M of NaCl and 0.3 M of Na_3-citrate; pH 7.2) for 30 min each. The slides were maintained in detection buffer 1 (0.1 M of Tris-HCl at pH 7.5 and 0.15 M of NaCl) for 5 min and then incubated in blocking buffer for 30 min. The sections were washed again in detection buffer sensing 1 for 5 min and incubated for 1 h with the antibody anti-Digoxigenin AP Fab Fragments (Roche®) diluted 1:1000 in detection buffer 1. Subsequently, two 15-min washes in detection buffer and a 5-min wash in detection buffer 3 (0.1 M Tris-HCl—pH 7.5, 0.1 M NaCl; 0.05 M MgCl2) were carried out. Sections were incubated in staining solution containing 4.5 μL of BCIP (5-bromo-4-chloro-3-indolyl-phosphate) (0.05 g mL^{-1}) and 4.5 μL of NBT (nitrobluetetrazolium) (0.05 g mL^{-1}) in 1 mL of buffer 3 for 45 min in the dark. The sections were incubated in detection buffer 4 (0.01 M of Tris-HCl at pH 8.0 and 1 mM of EDTA) for 10 min to stop the reaction, and the slides were mounted in water. Images was captured by an Olympus AX70TRF light microscope (Olympus Optical, Japan) equipped with a U-Photo system and coupled to a Zeiss AxioCam HRc digital camera.

Results

Development of embryogenic callus from immature zygotic embryo explant

To initially characterize the time course of the development of embryogenic callus in *B. distachyon*, we evaluated distinct phases of embryogenic development (Fig. 1). Immature zygotic embryo dissected 15 days after anthesis and used as explants was about 0.5 mm in width and consisted of large scutellum, coleoptile, and coleorhiza. The scutellum was attached to the embryo axis by the region between the coleorhiza and the coleoptile denominated scutellar node or mesocotyl. The coleoptile initiated from the adaxial surface of the scutellum and surrounded the first leaves. The coleorhiza, a conical sheath-like structure, was formed at the proximal end of the primary root. Two epiblasts arised just below the mesocotyl, each at the two opposite sides of the coleoptile base, and were continuous along with the scutellum (Fig. 1a, b).

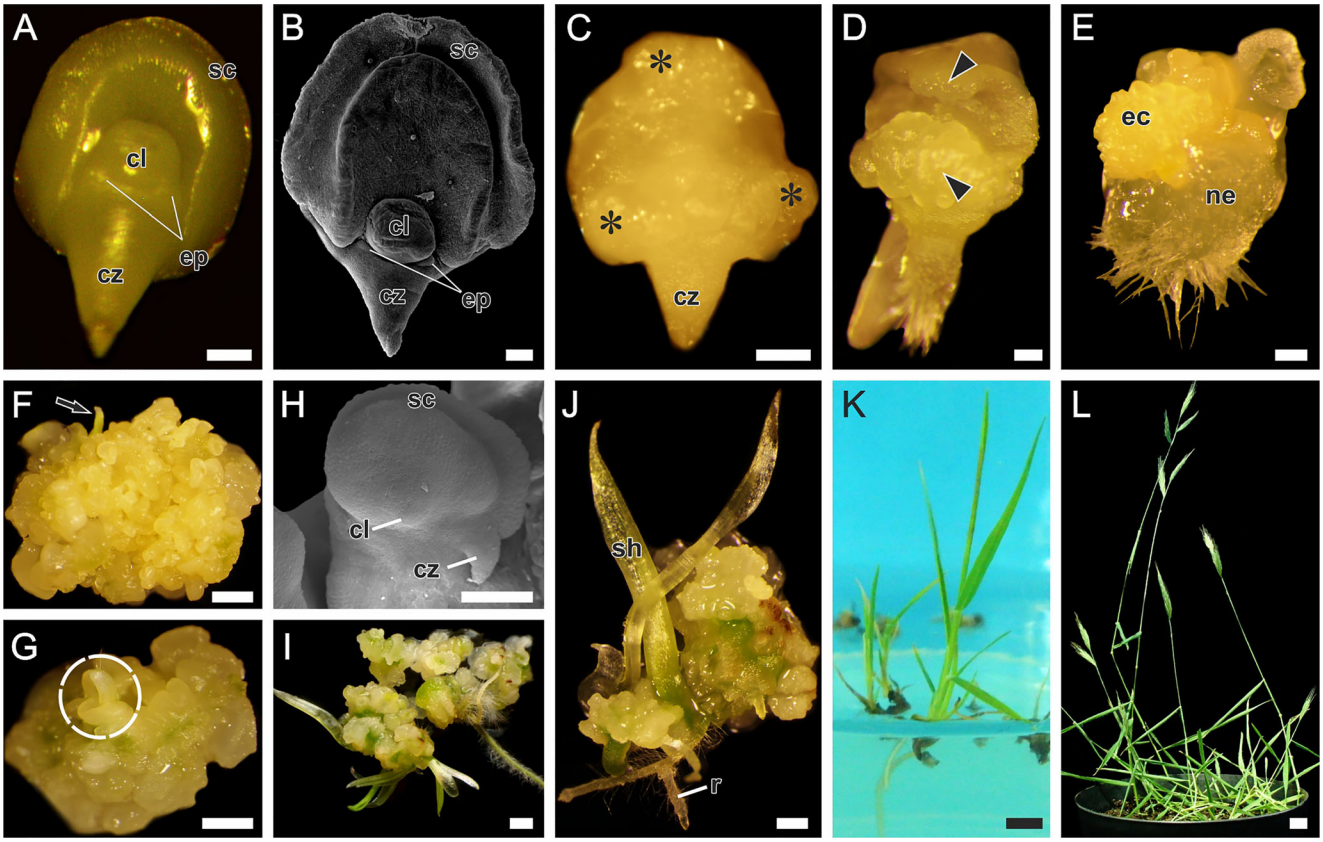

Fig. 1 Morphological view of the *Brachypodium distachyon* somatic embryogenesis process from immature zygotic embryo explants cultured on auxin-rich induction medium. **a**, **b** Micrographs of immature embryo 15 days post anthesis obtained from stereo microscope (**a**) and scanning electron microscopy (**b**). **c** Immature embryo at 3 days after culture. Bulges started to form on the surface of the edge of the scutellum (*asterisk*). **d** Callus formation (*arrowheads*). **e** Zygotic explants after 8 days of culture. A callus showing the differences between embryogenic (*ec*) and non-embryogenic callus (*ne*) areas. **f** Embryogenic callus after 10 days on regeneration medium showing somatic embryos at different developmental stages. *Arrow* indicates an aerial part of a somatic embryogenesis-derived shoot. **g** Embryogenic callus after 15 days on regeneration medium. Somatic embryo at the coleoptilar stage initiates germination (*white circle*). **h** Scanning electron micrograph showing well-developed somatic embryo attached to the subtending callus after 2 weeks on regeneration medium. **i** Regenerating embryos with coleoptiles directly coming from scutella after 15–21 days on regeneration medium. **j** Plantlet with well-defined shoot (*Sh*) and root (*r*) bipolar structure at 21 days on regeneration medium. **k** Regenerated plantlet developing roots 2 weeks after transfer to germination medium. **l** Regenerated plants after 6 weeks in compost mixture producing viable seeds. *cl* coleoptile, *cz* coleorhiza, *ec* embryogenic callus, *ep* epiblast, *ne* non-embryogenic callus, *sc* scutellum, *sh* shoot, *r* root. *Bars*: **a** 200 μm; **b**, **c**, **h** 100 μm; **d**, **e** 125 μm; **f**, **g** 250 μm; **i**, **j** 500 μm; **k** 5 mm; **l** 10 mm

During the first 2–4 days of culture, a progressive swelling of the scutellum and mesocotyl was observed. The coleorhiza and coleoptile started to elongate and epidermal hairs grew on the coleorhiza (Fig. 1c, d). After 6–8 days, a callus mass was formed on the scutellum surface (Fig. 1d). Proembryogenic clusters showed different morphological aspects in the non-embryogenic regions (Fig. 1e). Proembryogenic clusters presented a creamy-white color, a smooth surface, and a nodular appearance. In contrast, the non-embryogenic callus was friable and translucent with a rough surface (Fig. 1e).

The callus mass continued to proliferate and after 4 weeks of culture compact embryogenic calli were transferred onto the regeneration medium in the light and developed into well-formed, creamy-white scutella (Fig. 1f, g). Localized chlorophyll also occurred in some green regions of the callus (Fig. 1g). Coleoptiles emerged from the coleoptilar pore in the scutellum of fully developed somatic embryos (Fig. 1f, g). The developments of both coleorhiza and coleoptile were observed by SEM, indicating a bi-polarity of somatic embryo development (Fig. 1h). Somatic embryos germinated (Fig. 1i) and shoot-root axis grew in regeneration medium and developed green plantlets (Fig. 1j). Occasionally, root development was delayed and the plantlet remained connected to the callus or produced small roots. These plantlets further developed following subculture for 2–3 weeks on the germination medium (Fig. 1k). Rooted plants were successfully established in compost mixture, produced fertile flowers, and set viable seeds (Fig. 1l).

Histological and histochemical changes during embryogenic callus development

Next, we characterized histological changes in *B. distachyon* embryogenic calli. Given that the development of embryogenic calli started on scutellum surface, we performed longitudinal sections of embryos explants prior to in vitro culture. These sections revealed that the scutellar tissue is composed of a single protodermal layer, which in turn consists of dense cytoplasmic cells as well as a compact ground meristem tissue comprising relatively large parenchyma cells with dense cellular content (Fig. 2a). At the 3rd day of culture, the coleorhiza and coleoptile begun to elongate and clear anatomic modifications in the explants could be detected (Fig. 2b). Intense periclinal divisions were observed in the protodermal and subprotodermal cell layers in the scutellum (Fig. 2b, c). These edge cells were intensely stained and kept the cytological features that had been previously observed, such as dense cytoplasm and evident nucleus. On the other hand, ground meristem cells of inner layers begun to expand and exhibited a hyaline cytoplasm content and vacuolization (Fig. 2c). Further mitotic proliferation activity of scutellum protodermal cells led to callus-like structures in some regions of this tissue (Fig. 2d).

From 6 to 8 days, proembryogenic cell zones further developed through a continued series of complex cellular division pattern in the region corresponding to the embryogenic callus (Fig. 2e). The proembryogenic zones were attached to

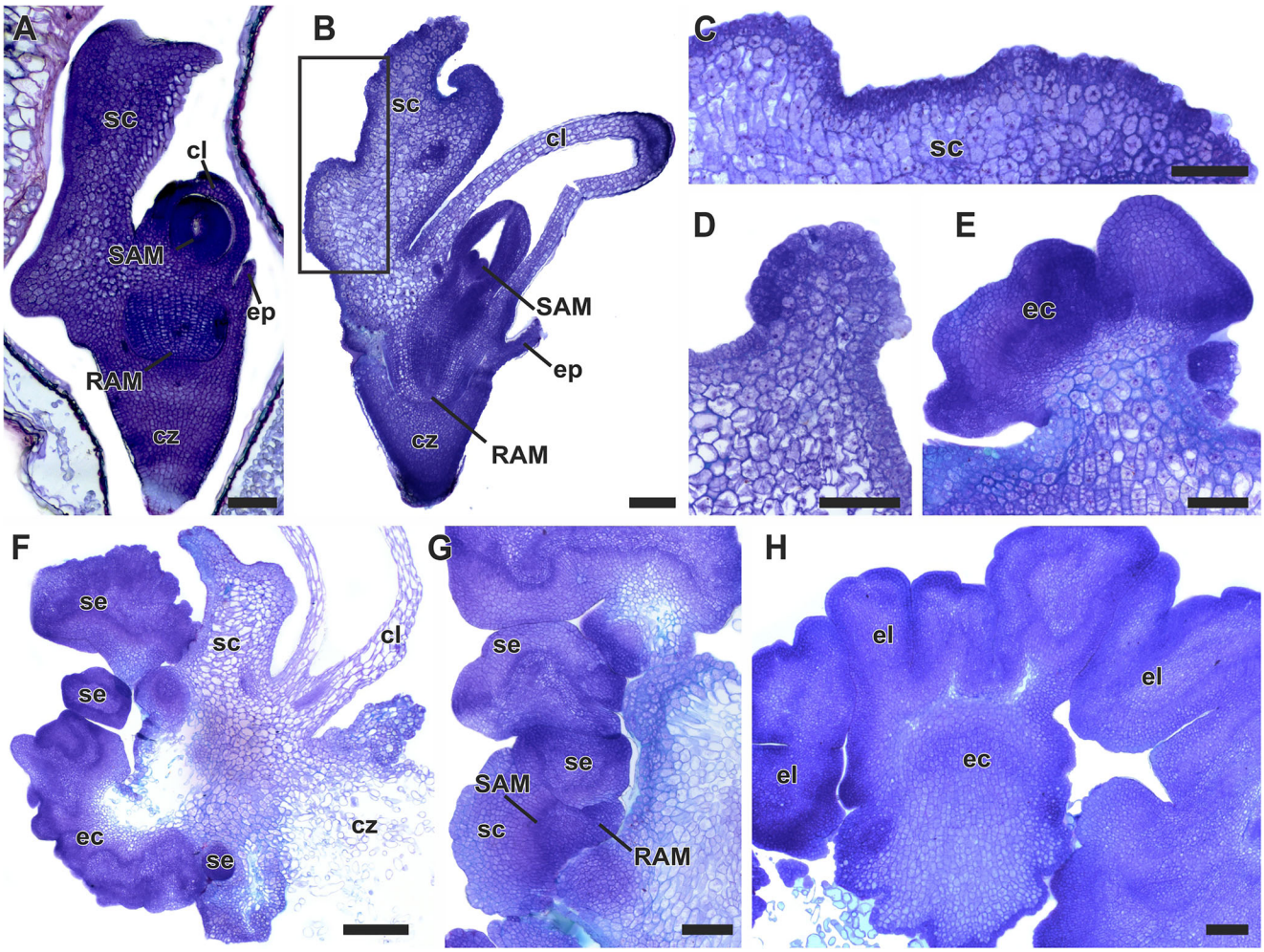

Fig. 2 Histological characterization of *Brachypodium distachyon* somatic embryogenesis process from immature zygotic embryo explants cultured on auxin-rich induction medium. Longitudinal sections. **a** Histological organization of initial zygotic embryo explant. **b**, **c** Explant after 3 days in SE induction medium. Note the dense cytoplasm of protodermal-dividing cells in comparison to hyaline cytoplasm of inner cell layers of the scutellum. **d**, **e** Early (**d**) and late (**e**) embryogenic callus (*ec*) formation. **f** Explant after 10 days of culture. Further development of the embryogenic callus lead to somatic embryo (*se*) formation that grew irregularly. **g** Somatic embryos (*se*) at different development stages showing the presence of shoot and root apical meristem, scutellum, and closed vascular system. **h** Densely stained compact embryogenic callus (*ec*) and embryo-like structures (*el*) completely separated from the original explant at 12 days of culture. *cl* coleoptile, *cz* coleorhiza, *ec* embryogenic callus, *el* embryo-like structures, *ep* epiblast, *RAM* root apical meristem, *SAM* shoot apical meristem, *sc* scutellum, *se* somatic embryo. *Bars*: **a**–**c** 200 μm; **d**, **e** 100 μm; **f** 500 μm; **g**, **h** 250 μm

the callus by a broad multicellular base (Fig. 2e). From 8 to 21 days of culture, the proembryogenic zones formed embryo-like structures composed of meristematic cell aggregates with closed vascular system. These structures showed a well-defined protoderm and were therefore identified as somatic embryos (Fig. 2f, g). At this stage, the establishment of the apical/basal polarity was observed by the development of shoot and root apical meristems in the somatic embryos (Fig. 2g). The establishment of adaxial/abaxial polarity axis of the somatic embryo was also possible, being recognized by scutellum formation (Fig. 2g). After 28 days of culture, embryogenic callus and embryogenic-like structures that were maintained in culture showed progressive growth and were completely separated from the original explant (Fig. 2h).

Histochemical tests were performed in the scutellum tissue region during SE induction (Fig. 3a–h). Starch grains were evidenced in the immature zygotic embryos used as initial explants by the positive reaction to PAS. Starch grains appeared uniformly distributed within the scutellum cells (Fig. 3a). No protein bodies were identified in the scutellum, even though a weak, uniform positive reaction to Xylidine Ponceau (XP) was observed in the scutellum tissue, evidencing the presence of structural proteins (Fig. 3b).

After 4 days in the SE induction medium, starch granules were less abundant than those at the initial stage. The formers were mostly present in the inner cell layers of the scutellum, region which was not involved in the regeneration process. Starch granules were not evident throughout the division of embryogenic callus cells (Fig. 3c). A different response reaction to XP was observed between the scutellum regions that were involved and not-involved in callus formation. Protodermal cells that actively divided to form the embryogenic callus showed a more intense stain in comparison to inner cell layers (Fig. 3d).

After 12 days of culture, similar stain pattern was observed during the development of embryogenic-like structures (Fig. 3e, f). However, after 21 days, small starch granules became abundant and appeared scattered throughout the cells of embryogenic clusters (Fig. 3g). In addition, an intense XP stain was observed in this embryogenic zone (Fig. 3h).

The Sudan Black test was negative for lipids in the initial explant as well as throughout the SE pattern (data not shown).

Cytological changes during embryogenic callus differentiation

The scutellum tissue of immature zygotic embryos explants were originally composed by cells with numerous starch granules and a dense cytoplasm, but some of these became progressively vacuolated (Fig. 4a, b). The nucleus was overall centrally located, possessing a nucleolus (Fig. 4a, b). Mitochondria and rough endoplasmic reticulum were already evident and differentiated (Fig. 4b).

After 4 days of culture, mitotic activity was observed first in periphery scutellum cells (Fig. 4c). The protoplasm of scutellum periphery cells retained the same cytological features that had been previously observed. Mitochondria, Golgi apparatus, rough endoplasmic reticulum, and free ribosomes were distributed within the cytoplasm (Fig. 4c, d). Amyloplasts with starch granules accumulation were also observed. However, starch granules became fewer and smaller (Fig. 4d) when compared to the initial stage (Fig. 4a, b).

After 12 days of culture, proembryogenic zones of outer callus cells origin were observed (Fig. 4e). These proembryogenic cells were in an intense mitotic activity. The cell walls that were formed between daughter cells were relatively thin (Fig. 4e–g). Usually, proembryos cells presented meristematic characteristics, being composed by a central, evident nucleus as well as a dense cytoplasm that primarily contained free ribosomes, a Golgi apparatus, mitochondria, and rough endoplasmic reticulum, which was randomly distributed (Fig. 4f, g). The nucleus of each embryogenic cell contained only one prominent nucleolus and small heterochromatin regions (Fig. 4f). In the cytoplasm, the Golgi apparatus was randomly distributed throughout the cytoplasm and was composed of cisterns that actively produced dictyosomal vesicles (Fig. 4g). In these cells, the vacuole component was reduced and starch granules were practically absent. Plasmodesmata could be observed between the walls of neighboring cells of the newly divided embryogenic cells (Fig. 4g).

Identification and characterization of *B. distachyon SERK* genes

The search for results concerning the latest release of *B. distachyon* genome (v3) on the Phytozome database revelead the presence of at least three putative *SERK* homologs: two annotated as *BdSERK*1 (Bradi3g46747 and Bradi5g12227) and one Bradi3g15660 available on Phytozome as a putative leucine-rich repeat protein kinase, subfamily LRRII, but showing 100% of identity with a sequence named as BdSERK2 (LOC100834508) in NCBI. Bradi3g46747 was located in chromosome 3 with a predicted mRNA (Bradi3g46747.1) of 2754 bp and ORF of 627 amino acids (pI/Mw 5.49/68.8 KDa). The Bradi5g12227 sequence was identified as part of chromosome 5, with mRNA sequence of 2471 bp encoding an ORF of 630 amino acids (pI/Mw 5.78/69.7 KDa). The comparison of the predicted amino acid sequences of both ORFS related to *SERK1* gene demonstrated 91% of identity and 93% of similarity.

BdSERK2 corresponded to locus Bradi3g15660 present on chromosome 3. The mRNA sequence (Bradi3g15660.2) has 2458 bp and a predicted amino acid sequence of 625 amino acids (pI/Mw 5.65/68.7 KDa). All sequences shared a conserved exon-intron structure composed of 11 exons and 10 introns.

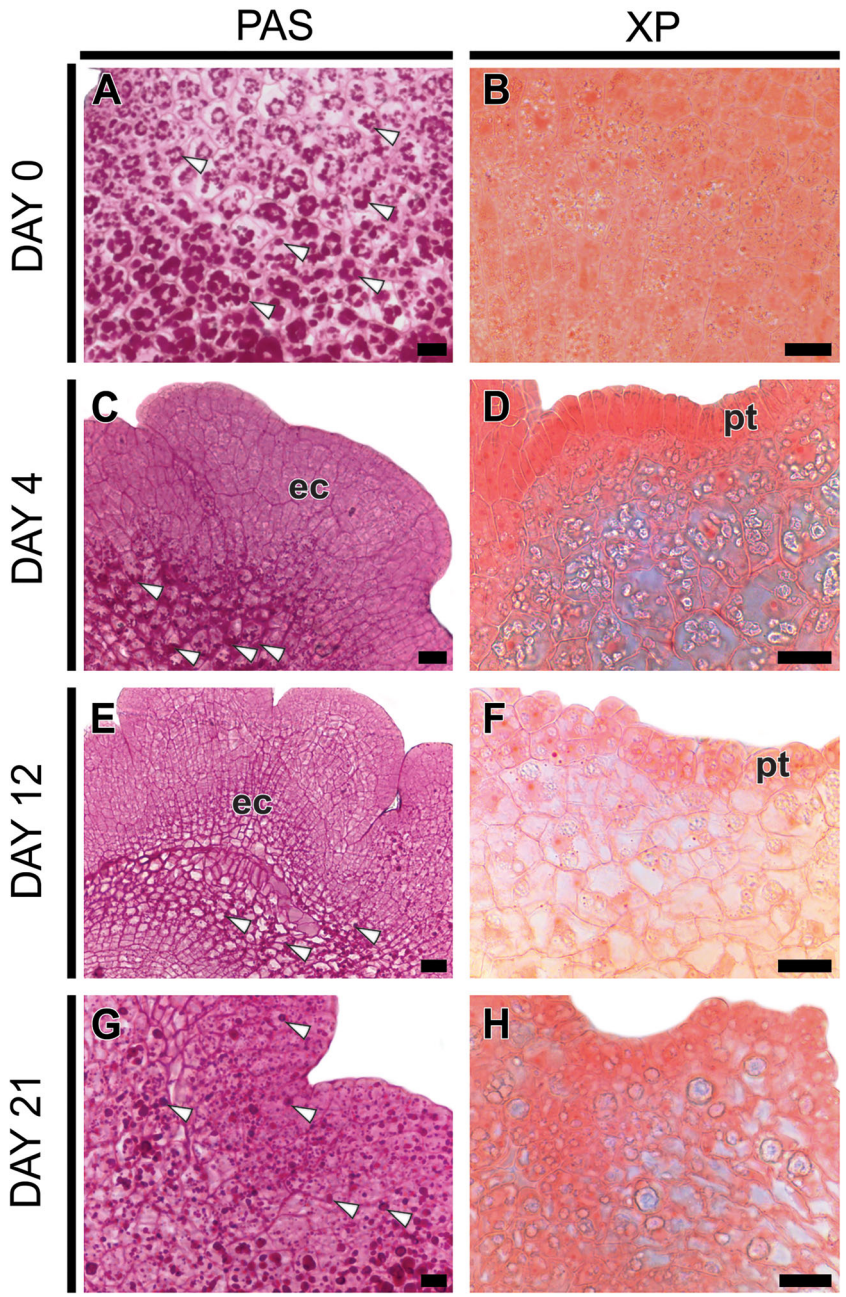

Fig. 3 Histochemical characterization of *Brachypodium distachyon* somatic embryogenesis process from immature zygotic embryo explants. Longitudinal sections of immature scutellum from 0 to 21 days after culture were subjected to staining with PAS (**a**, **c**, **e**, **g**) and Xylidine Ponceau (**b**, **d**, **f**, **h**). **a**, **b** Scutellum of immature zygotic embryo. **a** Positive reaction for starch (*white arrowheads*). **b** A faint positive reaction for total proteins. **c**, **d** Scutellum after 4 days in induction media. **c** Starch content only in the inner cell layers (*white arrowheads*). **d** A strong positive XP-staining in protodermis-dividing cells (*pt*). **e**, **f** Embryogenic callus after 12 days in induction media. **g**, **h** Embryogenic callus after 21 days in induction media. **g** Positive reaction for starch **(g)** and total proteins **(h)** in embryo-like structures. *ec* embryogenic callus, *pt* protodermal cells. *Bars* 25 μm

Analysis of BlastN and BlastP of the three homologs mentioned against Non-redundant databank of NCBI revealed identities ranging between 83and 94% with SERK1/SERK2 homologs of other grasses, namely *T. aestivum*, *O. sativa*, *Sorghum bicolor*, *Setaria italica*, and *Z. mays*.

CDD and Pfam analyses revealed the presence of structural domains that are characteristic of *SERK* protein, being an extracellular domain that contains a signal peptide followed by a leucine Zipper motif, 5 leucine-rich repeat (LRR1-LRR5), a rich proline motif (SPP), a transmembrane domain, and the intracellular kinase domain followed by C-terminal. Putative signal peptides were predicted from amino acid sequences for the three BdSERK homologs. For Bradi3g46747.1, it was detected a cleavage site between positions 29 and 30. However, for Bradi5g12227.1, no cleavage site was detected within the signal peptide region. For BdSERK2 (Bradi3g15660.2), a cleavage site was detected between positions 25 and 26 (Fig. S1). The multiple sequence alignments (MSA) showed that the functional domains were overall well-conserved in relation to SERK1/SERK2 homologs of other monocots. Substitutions of amino acids and a few gaps were observed in all sequences, being the signal peptide and region between the SPP motif and transmembrane domain, the less conserved.

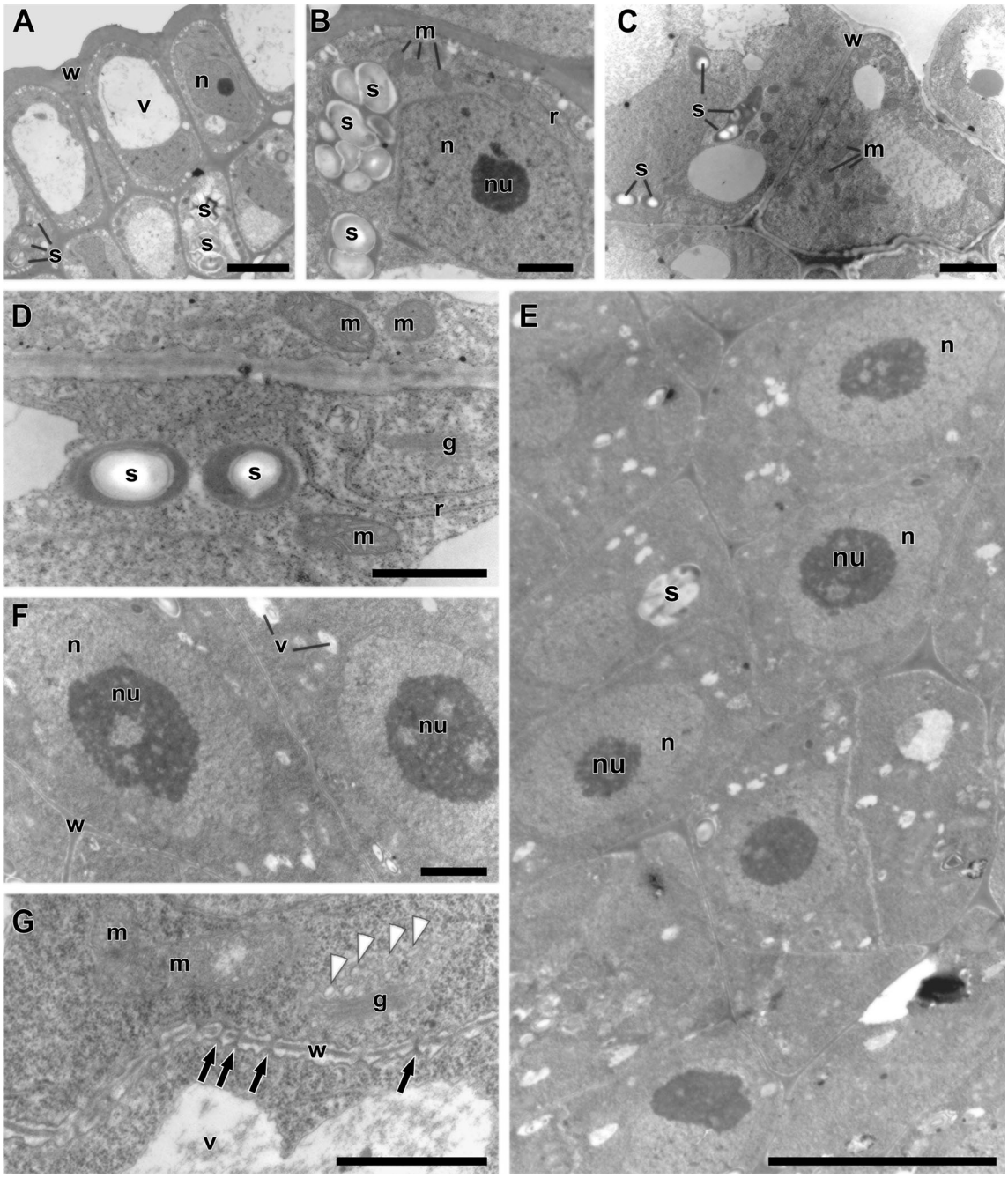

Fig. 4 Cytological changes involved in embryogenic callus differentiation from scutellum of *Brachypodium distachyon* zygotic embryo explants. **a**, **b** Scutellum cells of the initial explant. Note the cellular organization with an evident nucleus (*n*) and starch granules (*s*). **c**, **d** Four days of culture. Note anticlinal division pattern (**c**), the dense cytoplasm and the small starch granules (**d**). **e**–**g** At 12 days of culture. **e** General view of proembryogenic zone. **f** Detail of the large nucleus (*n*) showing with a conspicuous nucleolus (*nu*) and small regions of heterochromatin. **g** Dense cytoplasm with well-differentiated organelles as mitochondria (*m*), Golgi apparatus (*g*) producing dictyosomal vesicles (*white arrowheads*) and plasmodesmata (*arrows*) distributed throughout the newly formed cell walls (*w*). g Golgi apparatus, *r* endoplasmic reticulum, *m* mitochondria, *n* nucleus, *nu* nucleolus, *v* vacuole, *w* cell wall, *s* starch. *Bars*: **a**, **e** 5 μm; **c** 2 μm; **b**, **d**, **f**, **g** 1 μm

The rooted phylogenetic summary constructed from the alignment of deduced amino acid using NJ method showed a close relationship between the predicted protein of *B. distachyon* and members of SERK family of other grasses, including *S. italica*, *S. bicolor*, *Z. mays*, and *T. aestivum* (Fig. 6). A more complete alignment analysis involving 65 SERK proteins of different taxa, including eudicots, monocots, and non-vascular plants as well as four non-SERKs kinase proteins used as external group showed BdSERK homologs grouped together to the class of *SERK1/2* of monocots (Fig. S2).

Furthermore, the conservation score, determined by Consurf algorithm for both BdSERK1 (Bradi5g12227.1) and

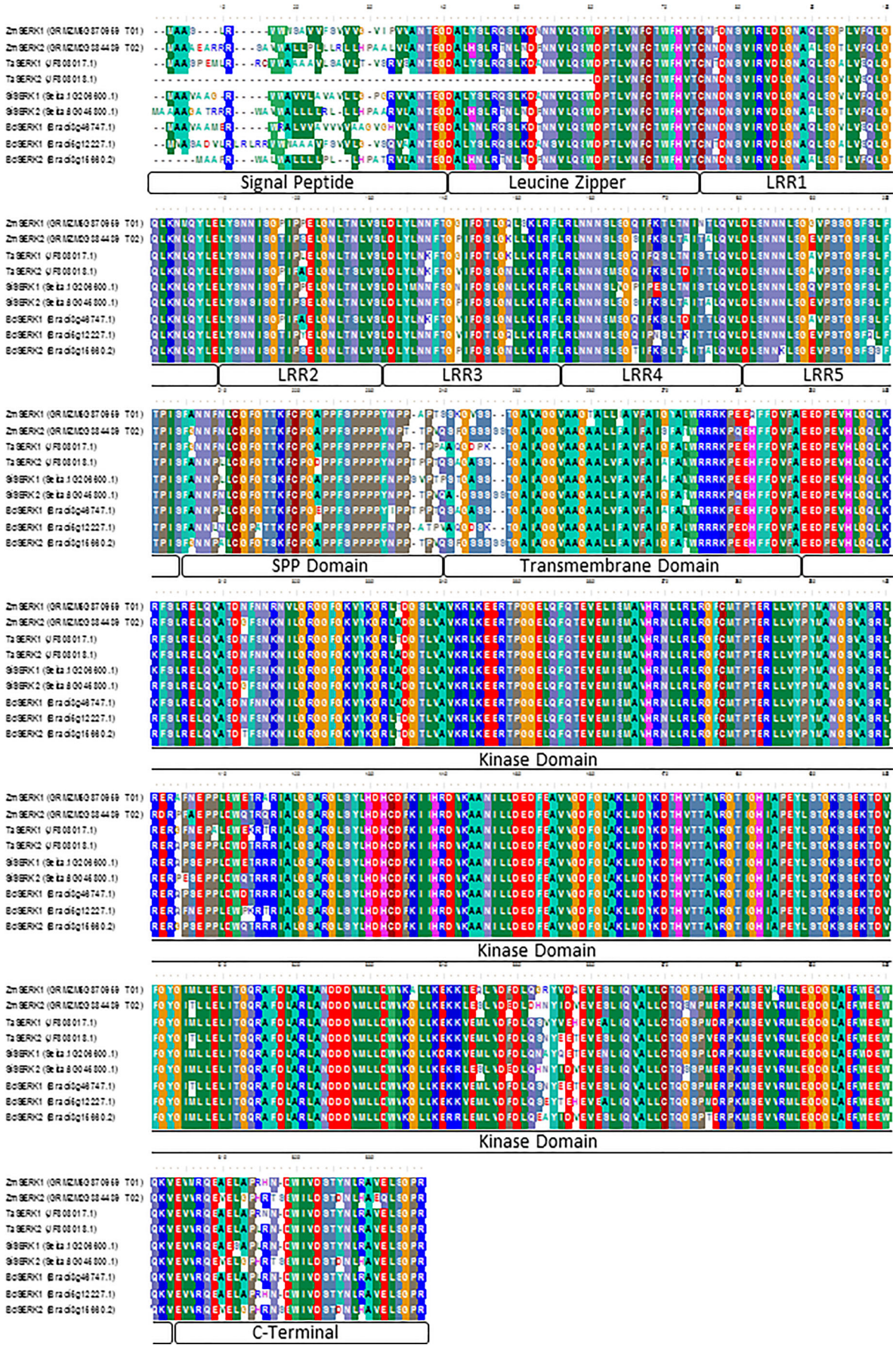
Signal Peptide
Leucine Zipper
LRR1
LRR2
LRR3
LRR4
LRR5
SPP Domain
Transmembrane Domain
Kinase Domain
Kinase Domain
Kinase Domain
C-Terminal

◀ **Fig. 5** Sequence alignments of SERK-like proteins with other monocot species with *B. distachyon* SERK, showing the high similarity of the SERK protein structural domains. The deduced amino acid sequences of SERK proteins were aligned, and amino acids differing from the consensus are colorless. Below the sequences, the protein domains are indicated by *rectangles*: *SP* signal peptide, *ZIP* leucine zipper, *LRR* leucine-rich repeats, *SPP* proline-rich region, *TM* transmembrane domain, *Kinase* protein-kinase domain, *C C*-terminal domain

BdSERK2 (Bradi3g15660.2), and plotted onto 3D structure of the LRR-extracellular domain, demonstrated a high conservation state of the concave side of interaction ligand receptor (Fig. 7a, b), in comparison to the convex side (solvent exposed) (Fig. 7c, d). However, some amino acid positions of BdSERK-LIKE 2, marked in light yellow, denoted a conservation level with low confidence due to insufficient data for analysis (Landau et al. 2005).

Localization of *B. distachyon BdSERK-1* transcripts during the somatic embryogenesis

Transcripts of *BdSERK1* were present in all tissues of the immature zygotic embryos used as initial explants (Fig. 8a) and throughout the whole culture period in somatic embryogenesis induction medium (Fig. 8b–d). After 2 days in induction medium, a hybridization signal was observed in the entire embryo axis and in the scutellum. A stronger signal was detected in the scutellum periphery, where mitotic divisions occurred (Fig. 8b). After 12 days of culture, results from in situ hybridization showed that spatial expression of *B. distachyon SERK1* occurred mainly in callus regions that contained meristematic zones (Fig. 8c). From 12 to 21 days of culture, expression signals were also detected in embryos at different developmental stages. At 21 days of culture, *SERK* transcripts were kept in the meristematic cells of the compact embryogenic calli and somatic embryos (Fig. 8d). Sense probe did not generate characteristic hybridization signal (Fig. 8e).

Discussion

We showed that immature *B. distachyon* zygotic embryos cultured on auxin-rich induced medium were sufficient to determine the reprogramming process required for cell-fate transition involved in SE. Although SE has been previously reported for *B. distachyon* (Ye and Tao 2008), we provided here new insights to better understand the basic cellular and molecular mechanisms that underlie the SE process of grass species. The main developmental features presented in this paper are discussed below.

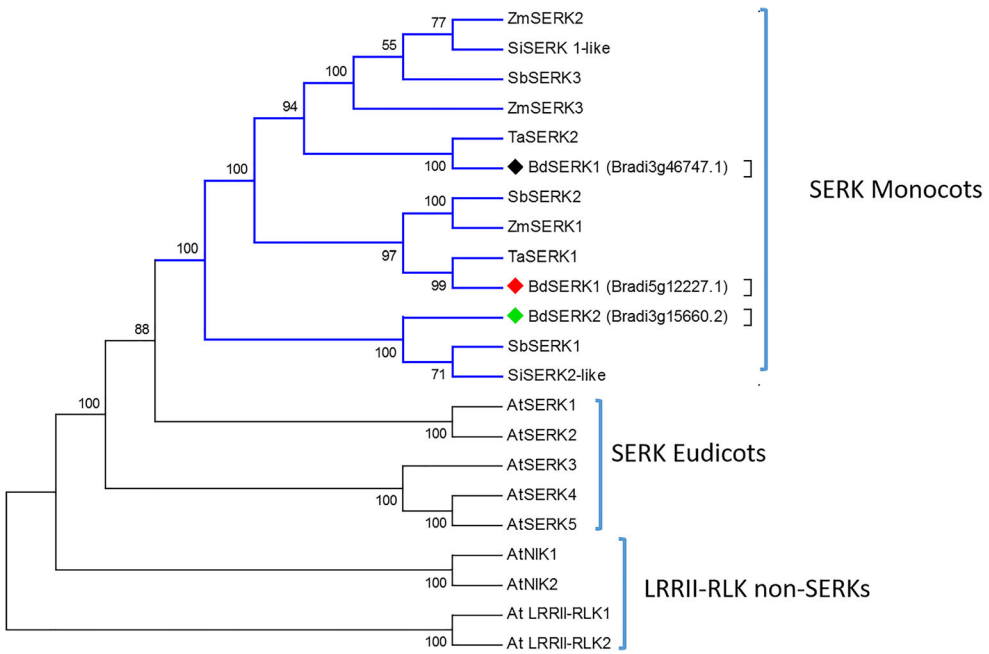

Fig. 6 Phylogenetic relationship of SERK proteins. The evolutionary history was inferred using the neighbor-joining method (Saitou and Nei, 1987). The optimal tree with the sum of branch length = 4.23739800 is shown. The percentage of replicate trees in which the associated taxa clustered together in the bootstrap test (1000 replicates) are shown next to the branches (Felsenstein 1985). The evolutionary distances were computed using the Dayhoff matrix based method and are in the units of the number of amino acid substitutions per site (Schwarz and Dayhoff, 1979). The analysis involved 21 amino acid sequences, available at Genbank. All positions containing gaps and missing data were eliminated. There were a total of 692 positions in the final dataset. Evolutionary analyses were conducted in MEGA7 (Kumar et al. 2016)

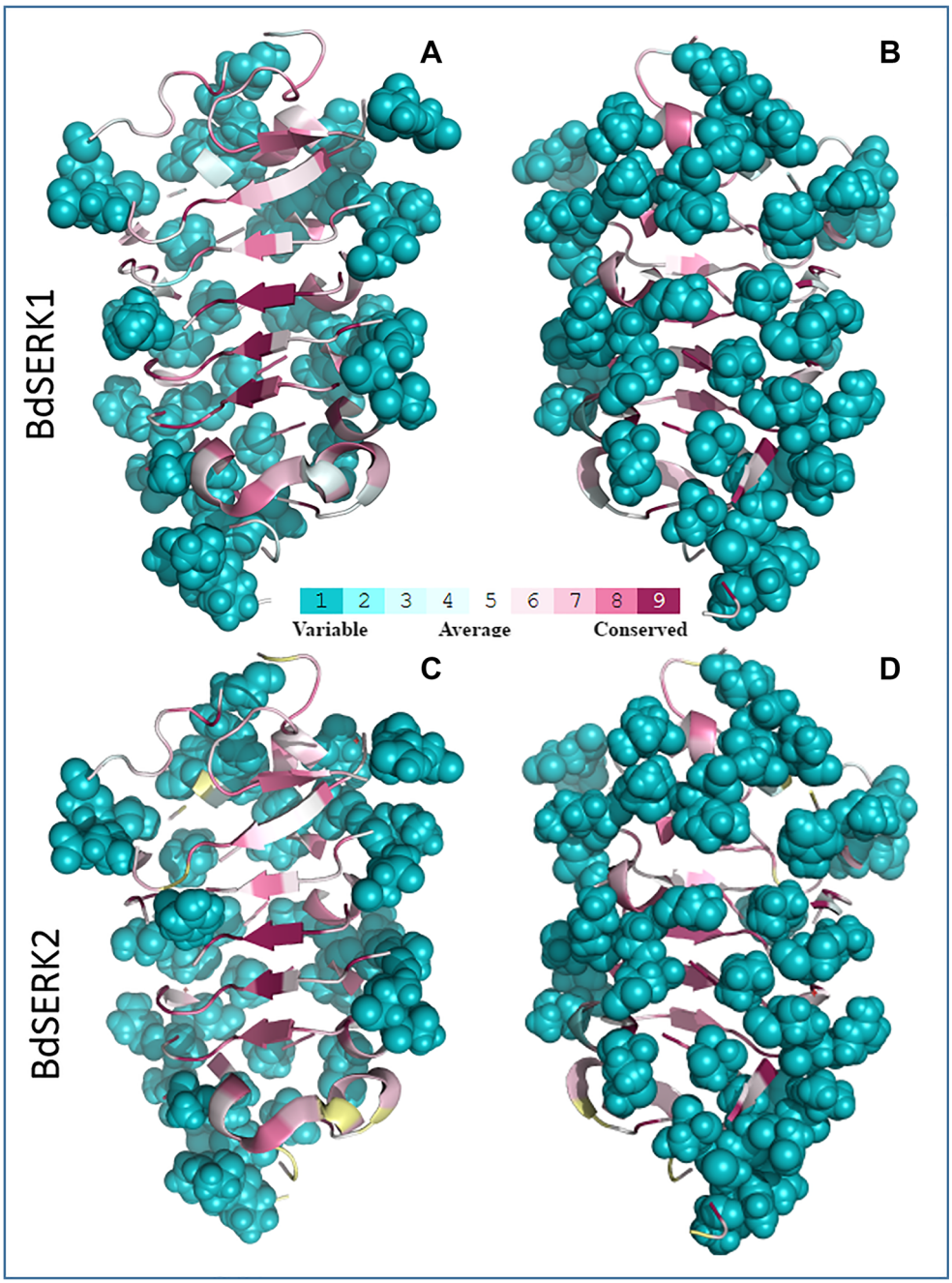

Fig. 7 Conservation score of the amino acids sequences in the LRR-extracellular domain in BdSERK1 and BdSERK2. The analysis was performed using ConSurf algorithm (Ashkenazy et al. 2010) from multiple alignment of the BdSERK sequences with other 65 SERK homologs and plotted onto the reported structure of the SERK1 ectodomain (PDB: 4LSC; Santiago et al. 2013). Scores plotted as *red-violet* onto the structure, represent residues of higher conservation, whereas that less conserved residues are indicated by *cyan*. Scores in *light yellow* denoted a conservation level with low confidence. **a**, **c** Concave side (interaction site with ligand receptors) in BdSERK1 (**a**) and BdSERK2 (**c**). **b**, **d** Convex side (solvent exposed) in both BdSERK proteins

Scutellum protodermis is intrinsically prone to undertake morphogenic pathways in grass

Morpho-histological observations during SE developmental process of *B. distachyon* showed the formation of embryogenic callus initiated at the scutellum (Figs. 1 and 2). Interestingly, the morphogenic responses obtained from zygotic embryo explants started from cotyledons in eudicots (Canhoto and Cruz 1996; Moura et al. 2008; Pinto et al. 2010; Rocha et al. 2012, 2016) or scutellum in monocots (Taylor and Vasil 1996; Nonohay et al. 1999; Lenis-Manzano et al. 2010; Delporte et al. 2014; Liu et al. 2015) in almost all developmental studies reported in literature. Scutellum is a unique structure in grass embryos and is considered by many to be a single cotyledon that does not emerge above ground (Chandler 2008). The grass scutellum and eudicot cotyledon play equivalent reserve roles in lipid, protein, and starch storage organs (Vernoud et al. 2005; Chandler 2008). Considering the homology between monocot and eudicot cotyledons, it seems that cotyledon is intrinsically prone to undertake morphogenic pathways and this feature is conserved between eudicots and monocots. However, the reason why cotyledon is a responsiveness organ

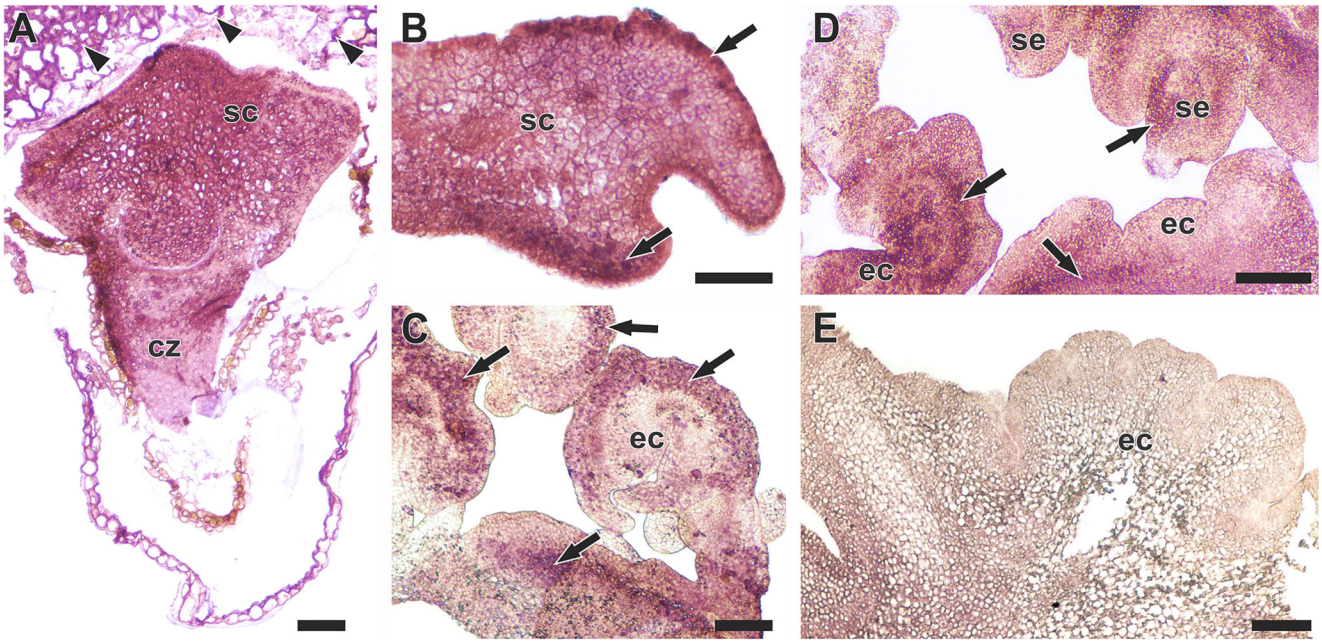

Fig. 8 Spatial localization of *SERK* gene in *Brachypodium distachyon* line Bd21 during somatic embryogenesis. **a** Initial zygotic embryo explant with hybridization signal in all its extension and in cells of the endosperm (*arrowheads*) of the immature seed. **b** Cells of the scutellum protodermis at 2 days of culture com strong hybridization signal (*arrows*). **c** Section of embryogenic callus showing strong hybridization signal in meristematic zones (*arrows*). A strong signal in the periphery of the scutellum of the proembryogenic zone (*arrows*). **d** Longitudinal section of compact callus showing strong hybridization signal in zones of meristematic cells and somatic embryos (*arrows*). **e** Section hybridized with the sense probe. No signal above background was detected. *cz* coleorhiza, *ec* embryogenic callus, *sc* scutellum, *se* somatic embryo. *Bars*: **a**–**c** 100 μm; **d**, **e** 200 μm

is still poorly understood. Recent data suggest that reserve compounds stored in cotyledons may have an important function during in vitro morphogenesis (Cangahuala-Inocente et al. 2004, 2009; Rocha et al. 2012; Moura et al. 2010; Silva et al. 2015). Furthermore, the large size difference between the cotyledon and the embryo axis as well as the closer contact between scutellum and the induction medium, make this structure more prone to perceive hormonal signaling that trigger regeneration, especially at its peripheral cell layers. These observations are consistent with recent reports on the molecular regulation during somatic embryogenesis in *Arabidopsis*, a model eudicot species, which showed the establishment of auxin gradients and the formation of morphogenetic responses in explant edge regions (Kurczyńska et al. 2007; Su et al. 2009). Auxin is known to play a key role in SE induction (Fehér et al. 2003; Yang and Zhang 2010; Rocha and Dornelas 2013). An accumulation of this plant growth regulator was identified in cotyledons dividing protodermal cells of *Arabidopsis* zygotic embryo explants during the first days of SE induction (Kurczyńska et al. 2007). These authors defined this features, auxin accumulation and population of protodermal-dividing cells, as the first signs of competence acquisition, stage at which a given cell or tissue assumes a new developmental fate.

Similarly, we interpreted the initial mitotic activity observed in the edge cells of the *B. distachyon* scutellum that could be formed by similar auxin-dependent mechanism (Fig. 2b, c). The meristematic features that we described in edge cells during the initial stages of *B. distachyon* SE, such as high division cell rate, dense cytoplasm, small vacuoles, and numerous mitochondria (Fig. 4c, d) also corroborate our hypothesis that dividing protodermal cells may represent a histocytological marker of competence acquisition in this regeneration system. Competence acquisition has been attributed to cells showing meristematic traits during the induction phase of the SE pathway (Fehér et al. 2003; Quiroz-Figueroa et al. 2006; Namasivayam 2007). Those anatomical and ultrastructural characteristics suggested their potential to proliferate and differentiate; as we have observed here the meristematic proliferation of protodermal cells gave rise to the embryogenic callus.

The differentiation of embryogenic calli from *B. distachyon* zygotic embryo explants is associated with the mobilization of starch storage reserve

B. distachyon scutellum cells exhibited a starch-rich content (Fig. 3a) that is consistent with the common reserve storage pattern described for monocot species (Bewley and Black 1994; Tomlinson et al. 2003; Guillon et al. 2011; Opanowicz et al. 2011). Starch forms the major storage product of grass and cereals (Bewley and Black 1994). It has been considered a primary source of energy for cell growth and proliferation during plant morphogenetic events (Martin et al. 2000;

Bewley and Black 1994). In this context, the reduction of starch granules observed in dividing protodermal cells at the initial developmental stages of *B. distachyon* SE pathway (Figs. 3c and 4d) suggests that these were required for embryogenic callus development. This hypothesis is also supported by the results obtained from XP-staining (Fig. 3d), which indicated a high protein content in protodermal cells involved in callus formation, at the same developmental stage. Starch grainules were no longer evident in those cells, suggesting an incidence of RNA synthesis and high metabolic activity in protodermal cells related to embryogenic callus formation.

At late stages, an increase in starch granules was observed in embryogenic-like structures (Fig. 3g), indicating an accumulation of this reserve compound in somatic embryos, as observed in *B. distachyon* zygotic embryos. It might be a result of cellular metabolism modification as a consequence of high sucrose levels used in the culture medium (Pinto et al. 2010). A high starch amount has been observed during the formation of somatic embryos in different species (Verdeil et al. 2001; Quiroz-Figueroa et al. 2002; Moura et al. 2008; Pinto et al. 2010). Although some studies have focused on the association between starch accumulation/consumption and somatic embryos formation, the possible function of this reserve compound in SE process remains unclear.

Differentiation and development of *B. distachyon* somatic embryos

The periphery of the proliferating callus tissue was more prone to give rise to regenerating structures. The formation of somatic embryos and embryo-like structures was preceded by the differentiation of proembryogenic clusters that were composed by clumps of small cells with dense cytoplasm. These observations agree with previous histological characterizations of grass regeneration systems (Nonohay et al. 1999; Lenis-Manzano et al. 2010; Delporte et al. 2014). The proembryogenic stem-like cells (Fig. 4e–g) had an evident nucleus with a single large, proeminent nucleolus with most of the chromatin as eurochromatin. These cytological features are typical of embryogenic cells (Verdeil et al. 2007; Kurczyńska et al. 2012; Rocha et al. 2016). According to Verdeil et al. (2007), these features might be used to distinguish between meristematic and embryogenic stem-like cells. Other ultrastructural characteristics evident in *B. distachyon* proembryogenic stem-like cells were the presence of Golgi apparatus—which was active in the production of dictyosomal vesicles —high division cell rate and absence of reserve compounds. These observations indicate the high metabolic activity that characterize proembryogenic stem-like cell clusters (Canhoto and Cruz 1996; Namasivayam 2007; Rocha et al. 2016).

Although we have not strictly recognized the embryogenic developmental stages of monocot zygotic embryogenesis, the mature *B. distachyon* somatic embryos resembled morpho-histologically the zygotic embryos. They exhibited apical–basal and radial polarity as well as a distinct scutellum (Fig. 2g). Histologically, somatic embryos also showed closed provascular system and fissures (Fig. 2g, h) that indicated regions of embryo detachment. This is consistent with the SE regeneration pattern (Namasivayam 2007).

Characterization of *BdSERK* genes

Despite all the genomic resources available in the databases and the importance of this species as a model plant, so far there is little information on the molecular aspects that drive the expression of somatic embryogenesis in *B. distachyon*. In this work, we have characterized three putative homologs of the SERK family available at Phytozome and NCBI databanks, two of which corresponded to *SERK1* gene and one annotated as *SERK2* gene. The sequences were characterized as to gene structure, conservation degree of the sequences, and phylogenetic positioning regarding to different taxa. The comparison of the deduced amino acid sequences against non-redundant protein databank revealed a high identity of sequences with BdSERK1/SERK2 homologs of other grasses like *T. aestivum*, *Z. mays, S. italica, S. bicolor*, and *O. sativa*, to mention a few. These sequences have conserved characteristic structural domains of SERK family members (Fig. 5). The deduced amino acid sequence extracellular domain consists of a variable signal peptide N-terminal, followed by 5 leucine-rich repeat motifs, and a typical SPP motif that is absent in other LRR kinases (Fig. 5). Nonetheless, concerning signal peptide prediction, no cleavage site has been detected on the N-terminal portion of protein sequence in Bradi5g12227.1. The absence of the signal peptide suggested the occurrence of mutations in this region, possibly affecting post-translational processing and protein distribution. However, further studies are necessary to confirm these mutations and the transcriptional pattern of these genes as well. Nevertheless, both BdSERK1 proteins identified here are isoforms, being gene products localized in different cromossomes.

Based on the genomic information available in the databank, no sequence showing identity with SERK3/BAK1 or other member of the SERK family has been identified in *B. distachyon*, suggesting that these are the only homologs present in this species. Conversely, in other species of Poales—including *S. bicolor*, *Ananas comosus*, *Z. mays*, and *T. aestivum*—the presence of this gene has been reported. On the other hand, species within eudicots showing a variable number of members in this family have been reported: *Arabidopsis thaliana* with 5 members (*SERK1-SERK5*), *Medicago truncatula* (*SERK1-SERK6*), *Vitis vinifera*

(*SERK1-SERK3*), *Glycine max* (*SERK1-SERK2*), and *Populus trichocarpa* (*SERK1-SERK4*) (Hecht et al. 2001; Nolan et al. 2011; aan den Toorn et al. 2015), among others.

The phylogenetic analysis based on rooted trees constructed with other SERK homologs and non-SERK proteins showed a close relationship of BdSERK sequences with SERKS of other monocots, especially grasses (Fig. 6 and Fig. S2). The rooted phylogenetic three constructed with other 65 sequences annotated as SERK and also4 non-SERK proteins was consistent with results of aan den Toorn et al. (2015) and comprised five classes: SERK1/SERK2 Eudicots; SERK Monocots; SERK non-vascular plants; SERK3/SERK4 Eudicots; and LRRII-LRK non-SERKs. These results suggest that *BdSERK* genes can have their conserved functions throughout the development of this species and that differences on sequences between BdSERK members can be associated to divergent functions in *B. distachyon* (aan den Toorn et al. 2015).

Additionally, the conservation score obtained by Consurf Software and plotted on 3D structure of extracellular domain for both BdSERK1 (Bradi5g12227.1) and BdSERK2 (Bradi3g15660.2) demonstrated that the concave side (red-violet colored), described as a site of interaction between SERK1-Brassinolide-BRI1 (Santiago et al. 2013) and other possible ligands, was more conserved in relation to the convex side (exposed to solvent). The solvent-exposed convex side (cyan colored) was more variable, as observed for SERK protein belonging to monocot and eudicot classes (aan den Toorn et al. 2015; Rocha et al. 2016) (Fig. 7).

BdSERKs are expressed throughout the *B. distachyon* SE developmental program

The in situ hybridization results indicated that *BdSERK*1 transcripts were observed throughout the *B. distachyon* embryogenic pathway. Before the establishment of the embryogenic culture, *BdSERK1* transcripts were detected in all tissues of the immature zygotic embryo used as initial explant (Fig. 8a). The expression of *SERK* genes has been historically associated to embryogenic pathways (both somatic and zygotic embryogenesis). Some reports have also demonstrated, by in situ RT-PCR analysis, the expression of *SERK1* in immature zygotic embryos of other monocot species such as *Z. mays* (Zhang et al. 2011) and *S. cereale* (Gruszczyńska and Rakoczy-Trojanowska 2011). After 12 days of culture, the hybridization signal was intensified in dividing cells committed to form the initial callus tissue in scutellum edge regions (Fig. 8c), which may denote a difference on the morphogenetic potential of the tissues. Interestingly, this strong hybridization signal was observed in protodermal cells at the same developmental stage as those that acquired meristematic features. Competent cells typically originate from cells expressing *SERK* (Kwaaitaal and De Vries 2007; Namasivayam 2007; Yang and Zhang 2010).

BdSERK1 expression continued throughout the *B. distachyon* SE developmental program in regions undergoing cellular proliferation activity (Fig. 8c) prior to the differentiation of somatic embryos. The positive relationship between the expression of *SERK* genes and cellular proliferation activity seems to be conserved in different plant species (Nolan et al. 2009; Pérez-Nuñéz et al. 2009; Savona et al. 2012; Li et al. 2015). These results are in accordance with a more broad view of the actual *SERK1* role, which would be associated to cellular reprogramming for cell-fate switches (Nolan et al. 2009; Savona et al. 2012). According to Savona et al. (2012), *SERK* genes might be associated with the specification of pluripotent cells.

At late stages of *B. distachyon* SE developmental program, *BdSERK1* transcripts remained strongly present in proembryogenic zones subtending and somatic embryos at different developmental stages (Fig. 8d). This *SERK* expression pattern corroborates the results observed in immature zygotic embryo explant of *B. distachyon* and has also been observed in other species like *Dactylis glomerata* (Somleva et al. 2000), *Solanum tuberosum* (Sharma et al. 2008), *Citrus* (Ge et al. 2010), *Z. mays* (Zhang et al. 2011), and *Trifolium nigrescens* (Pilarska et al. 2016). Conversely, expression signals in *SERK* gene expression in *Daucus carota* (Schmidt et al. 1997) and *Cocos nucifera* (Pérez-Nuñéz et al. 2009) ceased after the globular stage. Apparently, at late stages of somatic embryos differentiation, *SERK* genes expression does not have a conservative expression pattern during embryo developmental stages among the species.

In this work, we present the first report of *SERK* gene expression during somatic embryogenesis in *B. distachyon.* Because of limited material, quantitative gene expression assays were not possible. Further studies are needed for better understanding of *BdSERK* functions during induction and somatic embryo development, as well other physiological responses.

In summary, we showed new insights on morpho-histological, histochemical and molecular aspects into somatic embryogenesis from immature zygotic embryos of the model plant *B. distachyon* line Bd21. This study is the first to provide an integration of cellular and molecular data to describe the SE developmental program in this important model grass species. We believe that the results presented here might contribute to the understanding of the competence acquisition process as well as the development of somatic embryos in *B. distachyon*.

Acknowledgments This work was supported by the Conselho Nacional de Desenvolvimento Científico e Tecnológico (CNPq) (Brasília, DF, Brazil), Coordenação de Aperfeiçoamento de Pessoal de Nível Superior (CAPES) (Brasília, DF, Brazil), and Fundação de Amparo à Pesquisa do Estado de Minas Gerais (FAPEMIG) (Belo Horizonte, MG, Brazil). Caio G. Otoni is also acknowledged for the English revision.

Authors' contributions FTSN and WCO designed the research; EJO established the embryogenic cultures; ACFC, EJO, and LMV performed the light microscopy analysis; DIR and FAOT performed the scanning and transmission electron microscopy analyses; ADK, LMV, MVMP, EMM, and TCRS performed the characterization of sequences and in situ hybridization analysis; and ADK, DIR, EMM, EJO, FTSN, and WCO wrote the paper.

References

aan den Toorn M, Albrecht C, de Vries S (2015) On the origin of SERKs: bioinformatics analysis of the somatic embryogenesis receptor kinases. Mol Plant 8:762–782

Ashkenazy H, Erez E, Martz E, Pupko T, Ben-Tal N (2010) Consurf 2010: calculating evolutionary conservation in sequence and structure of proteins and nucleic acids. Nucleic Acids Res 38:529–533

Baudino S, Hansen S, Brettschneider R, Hecht VEG, Dresselhaus T, Lorz H, Dumas C, Rogowsky PM (2001) Molecular characterization of two novel maize LRR receptor-like kinases, which belong to the *SERK* gene family. Planta 213:1–10

Betekhtin A, Rojek M, Milewska-Hendel A, Gawecki R, Karcz J, Kurczyńska E, Hasterok R (2016) Spatial distribution of selected chemical cell wall components in the embryogenic callus of *Brachypodium distachyon*. PLoS One 11(11):e0167426

Bewley JD, Black M (1994) Seeds: physiology of development and germination. Plenum, London

Brisibe EA, Nishioka D, Miyake H, Taniguchi T, Maeda E (1993) Developmental electron microscopy and histochemistry of somatic embryo differentiation in sugarcane. Plant Sci 89:85–92

Brkljacic J, Grotewold E, Scholl R, Mockler T, Garvin DF, Vain P, Brutnell T, Sibout R, Bevan M, Budak H, Caicedo AL, Gao C, Gu Y, Hazen SP, Holt BF III, Hong SY, Jordan M, Manzaneda AJ, Mitchell-Olds T, Mochida K, Mur LAJ, Park CM, Sedbrook J, Watt M, Zheng SJ, Vogel JP (2011) *Brachypodium* as a model for the grasses: today and the future. Plant Physiol 157:3–13

Cabral GB, Carneiro VTC, Rossi ML, Silva JP, Martinelli AP, Dusi DMA (2015) Plant regeneration from embryogenic callus and cell suspensions of *Brachiaria brizantha*. In Vitro Cell Dev Biol—Plant 51: 369–377

Cangahuala-Inocente GC, Steiner N, Santos M, Guerra MP (2004) Morphological analysis and histochemistry of *Feijoa sellowiana* somatic embryogenesis. Protoplasma 224:33–40

Cangahuala-Inocente GC, Steiner N, Maldonado SB, Guerra MP (2009) Patterns of protein and carbohydrate accumulation during somatic embryogenesis of *Acca sellowiana*. Pesq Agropec Bras 44:217–224

Canhoto JM, Cruz GS (1996) Histodifferentiation of somatic embryos in cotyledons of pineapple guava (*Feijoa sellowiana* Berg.). Protoplasma 19:34–45

Chandler JW (2008) Cotyledon organogenesis. J Exp Bot 59:2917–2931

De Fillipis LF (2014) Crop improvement through tissue culture. In: Ahmad P, Wani MR, Azooz MM, Tran LSP (eds) Improvement of crops in the era of climate changes, 1st edn. Springer, New York, pp 289–346

Delporte F, Pretova A, du Jardin P, Watillon B (2014) Morpho-histology and genotype dependence of in vitro morphogenesis in mature embryo cultures of wheat. Protoplasma 251:1455–1470

Draper J, Mur LAJ, Jenkins G, Ghosh-Biswas GC, Bablak P, Hasterok R, Routledge APM (2001) *Brachypodium distachyon*. A new model system for functional genomics in grasses. Plant Physiol 127:1539–1555

Feder N, O'Brien TP (1968) Plant microtechnique: some principles and new methods. Am J Bot 55:123–142

Fehér A, Pasternak TP, Dudits D (2003) Transition of somatic plant cells to an embryogenic state. Plant Cell Tiss Organ Cult 74:201–228

Felsenstein J (1985) Confidence limits on phylogenies: an approach using the bootstrap. Evolution 39:783–791

Fitzgerald TL, Powell JJ, Schneebeli K, Hsia MM, Gardiner DM, Bragg JN, McIntyre CL, Manners JM, Ayliffe M, Watt M, Vogel JP, Henry RJ, Kazan K (2015) *Brachypodium* as an emerging model for cereal-pathogen interactions. Ann Bot 115:717–731

Fortes AM, Pais MS (2000) Organogenesis from internode-derived nodules of *Humulus lupulus* var. Nugget (Cannabinaceae): histological studies and changes in the starch content. Am J Bot 87:971–979

Ge XX, Fan GE, Chai LJ, Guo WW (2010) Cloning, molecular characterization and expression analysis of a *SOMATIC EMBRYOGENESIS RECEPTOR-LIKE KINASE* gene (*CitSERK1-like*) in Valencia sweet orange. Acta Physiol Plant 32:1197–1207

Girin T, David LC, Chardin C, Sibout R, Krapp A, Ferrario-Méry S, Daniel-Vedele F (2014) *Brachypodium*: a promising hub between model species and cereals. J Exp Bot 65(19):5683–5696. doi:10.1093/jxb/eru376

Gruszczyńska A, Rakoczy-Trojanowska M (2011) Expression analysis of somatic embryogenesis-related SERK, LEC1, VP1 and NiR ortologues in rye (*Secale cereale* L.). J Appl Genet 52:1–8

Guillon F, Bouchet B, Jamme F, Robert P, Quemener B, Barron C, Larre C, Dumas P, Saulnier L (2011) *Brachypodium distachyon* grain: characterization of endosperm cell walls. J Exp Bot 62:1001–1015

Hecht V, Vielle-Calzada JP, Hartog MV, Schmidt ED, Boutilier K, Grossniklaus U (2001) The *Arabidopsis SOMATIC EMBRYOGENESIS RECEPTOR KINASE 1* gene is expressed in developing ovules and embryos and enhances embryogenic competence in culture. Plant Physiol 127:803–816

Hu H, Xiong L, Yang Y (2005) Rice *SERK1* gene positively regulates somatic embryogenesis of cultured cell and host defense response against fungal infection. Planta 222:107–117

Karami O, Aghavaisi B, Pour AM (2009) Molecular aspects of somatic-to-embryogenic transition in plants. J Chem Biol 2:177–190

Karnovsky MJ (1965) A formaldehyde-glutaraldehyde fixative of high osmolality for use in electron microscopy. J Cell Biol 27:137–138

Kellogg EA (2015) *Brachypodium distachyon* as a genetic model system. Annu Rev Genet 49:1–20

Kumar S, Stecher G, Tamura K (2016) MEGA7: Molecular Evolutionary Genetics Analysis version 7.0 for bigger datasets. Mol Biol Evol 33: 1870–1874

Kurczyńska EU, Gaj MD, Ujczak A, Mazur E (2007) Histological analysis of direct somatic embryogenesis in *Arabidopsis thaliana* (L.) Heynh. Planta 226:619–628

Kurczyńska EU, Potocka I, Dobrowolska I, Kulinskalukaszek K, Sala K, Wrobel J (2012) Cellular markers for somatic embryogenesis. In: Sato KI (ed) Embryogenesis. InTech, Rijeka, pp 307–332

Kwaaitaal MACJ, De Vries SC (2007) The *SERK1* gene is expressed in procambium and immature vascular cells. J Exp Bot 58:2887–2896

Landau M, Mayrose I, Rosenberg Y, Glaser F, Martz E, Pupko T, Ben-Tal N (2005) Consurf 2005: the projection of evolutionary conservation scores of residues on protein structures. Nucleic Acids Res 33:299–302

Lenis-Manzano SJ, Araujo ACG, Valle CB, Santana EF, Carneiro VTC (2010) Histologia da embriogênese somática induzida em embriões de sementes maduras de *Urochloa brizantha* apomítica. Pesq Agropec Bras 45:435–441

Li X, Fang YH, Han JD, Bai SN, Rao GY (2015) Isolation and characterization of a novel SOMATIC EMBRYOGENESIS RECEPTOR KINASE gene expressed in the *fern Adiantum capillus-veneris* during shoot regeneration in vitro. Plant Mol Biol Rep 33:638–647

Liu B, Su S, Wu Y, Li Y, Shan X, Li S, Liu H, Dong H, Ding M, Han J, Yuan Y (2015) Histological and transcript analyses of intact somatic embryos in an elite maize (*Zea mays* L.) inbred line Y423. Plant Physiol Biochem 92:81–91

Mariani TS, Miyake H, Takeoka Y (1998) Changes in surface structure during direct somatic embryogenesis in rice scutellum observed by scanning electron microscopy. Plant Prod Sci 1:223–231

Martin AB, Cuadrado Y, Guerra H, Gallego P, Hita O, Martin L, Dorado A, Villalobos N (2000) Differences in the contents of total sugars, reducing sugars, starch and sucrose in embryogenic and non-embryogenic calli from *Medicago arborea* L. Plant Sci 29:143–151

Moura EF, Ventrella MC, Motoike SY (2010) Anatomy, histochemistry and ultrastructure of seed and somatic embryo of *Acrocomia aculeata* (Arecaceae). Sci Agric 67:399–407

Moura EF, Ventrella MC, Motoike SY, Sá Júnior AQ, Carvalho M, Manfio CE (2008) Histological study of somatic embryogenesis induction on zygotic embryos of macaw palm (*Acrocomia aculeata* (Jacq.) Lodd. ex Martius). Plant Cell Tiss Organ Cult 95:175-184

Murashige T, Skoog F (1962) A revised medium for rapid growth and bio assays with tobacco tissue cultures. Physiol Plant 15:473–497

Namasivayam P (2007) Acquisition of embryogenic competence during somatic embryogenesis. Plant Cell Tiss Organ Cult 90:1–8

Nolan KE, Irwanto RR, Rose RJ (2003) Auxin upregulates *MtSERK1* expression in both *Medicago truncatula* root-forming and embryogenic cultures. Plant Physiol 133:218–230

Nolan KE, Kurdyukov S, Rose RJ (2009) Expression of the *SOMATIC EMBRYOGENESIS RECEPTOR-LIKE KINASE1* (*SERK1*) gene is associated with developmental change in the life cycle of the model legume *Medicago truncatula*. J Exp Bot 60:1759–1771

Nolan KE, Kurdyukov S, Rose RJ (2011) Characterisation of the legume SERK-NIK gene superfamily including splice variants: Implication for development and defence. BMC Plant Biol 11:44

Nonohay JS, Mariath JEA, Winge H (1999) Histological analysis of somatic embryogenesis in Brazilian cultivars of barley, *Hordeum vulgare vulgare*, Poaceae. Plant Cell Rep 18:929–934

O'Brien TP, McCully ME (1981) The study of plant structure principles and selected methods. Termarcarphi Pty, Melbourne

Opanowicz M, Vain P, Draper J, Parker D, Doonan JHS (2008) *Brachypodium distachyon*: making hay with a wild grass. Trends Plant Sci 13:172–177

Opanowicz M, Hands P, Betts D, Parker ML, Toole GA, Mills EN, Doonan JH, Drea S (2011) Endosperm development in *Brachypodium distachyon*. J Exp Bot 62:735–748

Ozias-Akins P, Vasil IK (1982) Plant regeneration from cultured immature embryos and inflorescences of *Triticum aestivum* L. (wheat): evidence for somatic embryogenesis. Protoplasma 110:95–105

Pan X, Yang X, Lin G, Zou R, Chen H, Samaj J, Xu C (2011) Ultrastructural changes and the distribution of arabinogalactan proteins during somatic embryogenesis of banana (*Musa* spp. AAA cv. 'Yueyoukang 1'). Physiol Plant 142:372–389

Pearse AGE (1980) Histochemistry theoretical and applied. Churchill Livingston, Edinburgh

Pérez-Nuñéz MT, Souza R, Sáenz L, Chan JL, Zúñiga-Aguilar JJ, Oropeza C (2009) Detection of a *SERK*-like gene in coconut and analysis of its expression during the formation of embryogenic callus and somatic embryos. Plant Cell Rep 28:11–19

Petersen TN, Brunak S, Von Heijne G, Nielsen H (2011) Signal P 4.0: discriminating signal peptides from transmembrane regions. Nat Methods 8:785–786

Pilarska M, Malec P, Salaj J, Bartnicki F, Konieczny R (2016) High expression of SOMATIC EMBRYOGENESIS RECEPTOR-LIKE KINASE coincides with initiation of varius developmental pathways in vitro culture of *Trifolium nigrescens*. Protoplasma 253: 345–355

Pinto G, Silva S, Araújo C, Neves L, Santos C (2010) Histocytological changes and reserves accumulation during somatic embryogenesis in *Eucalyptus globulus*. Trees 24:763–769

Quiroz-Figueroa FR, Fuentes-Cerda CFJ, Rojas-Herrera R, Loyola-Vargas VM (2002) Histological studies on the developmental stages and differentiation of two different somatic embryogenesis systems of *Coffea arabica*. Plant Cell Rep 20:1141–1149

Quiroz-Figueroa FR, Rojas-Herrera R, Galaz-Avalos RM, Loyola-Vargas VM (2006) Embryo production through somatic embryogenesis can be used to study cell differentiation in plants. Plant Cell Tissue Organ Cult 86:285–301

Reynolds ES (1963) The use of lead citrate at high pH as an electron opaque stain in electron microscopy. J Cell Biol 17:208–212

Rocha DI, Dornelas MC (2013) Molecular overview on plant somatic embryogenesis. CAB Rev 8:1–17

Rocha DI, Vieira LM, Tanaka FAO, Silva LC, Otoni WC (2012) Somatic embryogenesis of a wild passion fruit species *Passiflora cincinnata* Masters: histocytological and histochemical evidences. Protoplasma 249:747–758

Rocha DI, Pinto DLP, Vieira LM, Tanaka FAO, Dornelas MC, Otoni WC (2016) Cellular and molecular changes associated with competence acquisition during passion fruit somatic embryogenesis: ultrastructural characterization and analysis of *SERK* gene expression. Protoplasma 253:595–609

Saitou N, Nei M (1987) The neighbour joining method: a new method for reconstructing phylogenetic trees. Mol Biol Evol 4:406–425

Santa-Catarina C, Hanai LR, Dornelas MC, Viana AM, Floh EIS (2004) *SERK* gene homolog expression, polyamines and amino acids associated with somatic embryogenic competence of *Ocotea catharinensis* Mez. (Lauraceae). Plant Cell Tiss Organ Cult 79:53–61

Santiago J, Henzler C, Hothorn M (2013) Molecular mechanism for plant steroid receptor activation by somatic embryogenesis co-receptor kinases. Science 341:889-892

Savona M, Mattioli R, Nigro S, Falasca G, Della Rovere F, Costantino P, De Vries S, Ruffoni B, Trovato M, Altamura MM (2012) Two SERK genes are markers of pluripotency in *Cyclamen persicum* Mill. J Exp Bot 63:471–488

Schmidt ED, Guzzo F, Toonen MA, Vries SC (1997) A leucine-rich repeat containing receptor-like kinase marks somatic plant cells competent to form embryos. Development 124:2049–2062

Schwarz R, Dayhoff M (1979) Matrices for detecting distant relationships. In Dayhoff M (ed) Atlas of protein sequences, National Biomedical Research Foundation. pp 353–358

Sharma SK, Millam S, Hein I, Bryan GJ (2008) Cloning and molecular characterization of a potato *SERK* gene transcriptionally induced during initiation of somatic embryogenesis. Planta 228:319–330

Silva GM, Cruz ACF, Otoni WC, Pereira TNS, Rocha DI, Silva ML (2015) Histochemical evaluation of induction of somatic embryogenesis in *Passiflora edulis* Sims (Passifloraceae). In Vitro Cell Dev Biol-Plant 51:539–545

Singla B, Khurana JP, Khurana P (2008) Characterization of three somatic embryogenesis receptor kinase genes from wheat, *Triticum aestivum*. Plant Cell Rep 27:833–843

Smertenko A, Bozhkov PV (2014) Somatic embryogenesis: life and death processes during apical-basal patterning. J Exp Bot 65: 1343–1460

Somleva MN, Schmidt EDL, De Vries SC (2000) Embryogenic cells in *Dactylis glomerata* L. (Poaceae) explants identified by cell tracking and by *SERK* expression. Plant Cell Rep 19:718–726

Spurr AR (1969) A low-viscosity epoxy resin embedding medium for electron microscopy. J Ultrastruct Res 26:31–43

Steiner N, Santa-Catarina C, Guerra MP, Cutri L, Dornelas MC, Floh EIS (2012) A gymnosperm homolog of *SOMATIC EMBRYOGENESIS RECEPTOR-LIKE KINASE*-1 (*SERK1*) is expressed during somatic embryogenesis. Plant Cell Tiss Organ Cult 109:41–50

Su YH, Zhao XY, Liu YB, Zhang CL, O'Neill SD, Zhang XS (2009) Auxin-induced *WUS* expression is essential for embryogenic stem cell renewal during somatic embryogenesis in Arabidopsis. Plant J 59:448–460

Taylor MG, Vasil IK (1996) The ultrastructure of somatic embryo development in pearl millet (*Pennisetum glaucum*; Poaceae). Am J Bot 83:28–44

Tomlinson K, Denyer K, Callow JA (2003) Starch synthesis in cereal grains. In: Callow JA (ed) Advances in botanical research. Academic, London, pp 1–61

Vain P (2011) *Brachypodium* as a model system for grass research. J Cereal Sci 54:1–7

Vasil V, Lu C, Vasil IK (1985) Histology of somatic embryogenesis in cultured immature embryos of maize (*Zea mays* L.). Protoplasma 127:1–8

Verdeil JL, Hocher V, Huet C, Grosdemange F, Escoute J, Ferriere N, Nicole M (2001) Ultrastructural changes in coconut calli associated with the acquisition of embryogenic competence. Ann Bot 88:9–18

Verdeil JL, Alemanno L, Niemenak N, Trambarger TJ (2007) Pluripotent versus totipotent plant stem cells: dependence versus autonomy? Trends Plant Sci 12:245–252

Vernoud V, Hajduch M, Khaled A-S, Depège N, Rogowski P (2005) Maize embryogenesis. Maydica 50:469–483

Vidal BC (1977) Acid glycosaminoglycans and endochondral ossification microespectrophotometric evaluation and macromolecular orientation. Cell Mol Biol 22:45–64

Vogel JP (2016) Plant genetics and genomics: crops and models, v. 18, Genetics and genomics of Brachypodium. Springer International Publishing, Heidelberg

Vogel J, Bragg J (2009) *Brachypodium distachyon*, a new model for the Triticeae. In: Feuillet C, Muehlbauer GJ (eds) Genetics and genomics of the Triticeae, vol 7, 1st edn. Springer-Verlag, New York, pp 427–449

Von Arnold S, Sabala I, Bozhkov P, Dyachok J, Filonova L (2002) Developmental pathways of somatic embryogenesis. Plant Cell Tiss Organ Cult 69:233–249

Wrobel J, Barlow PW, Gorka K, Nabialkowska D, Kurczyńska EU (2011) Histology and symplasmic tracer distribution during development of barley androgenic embryos. Planta 233:873–881

Yang X, Zhang X (2010) Regulation of somatic embryogenesis in higher plants. Crit Rev Plant Sci 29:36–57

Ye XG, Tao LL (2008) Research outline on some characteristics of *Brachypodium distachyon* as a new model plant species. Acta Agron Sin 34:919–925

Zhang S, Liu X, Lin Y, Xie G, Fu F, Liu H, Wang J, Gao S, Lan H, Rong T (2011) Characterization of a *ZmSERK* gene and its relationship to somatic embryogenesis in a maize culture. Plant Cell Tiss Organ Cult 105:29–37

Zimmerman JL (1993) Somatic embryogenesis: a model for early development in higher plants. Plant Cell 5:1411–1423